International Journal of Nanoelectronics and Materials
IJNeaM
ISSN 1985-5761 | E-ISSN 2232-1535

Characterization of SnO_2 Nanoparticles via *Morinda citrifolia* Leaf Extract

Irmaizatussyehdany Buniyamin[a,*], Mohd Yusri Idorus[b], Muhamad Faizal Abd Halim[a], Salifairus Mohammad Jafar[a], Zahidah Othman[a,c], Nur Fairuz Rostan[a,c], Kevin Alvin Eswar[a,d], Mohd Khairil Adzhar Mahmood[e], Maryam Mohammad[a,f], Mohamad Azri Tukimon[g], Hanis Mohd Yusoff[h,i], A. F. M. Motiur Rahman[j], Mohamad Rusop Mahmood[k], and Mohd Firdaus Malek[a,c]

[a]*NANO-SciTech Laboratory, Centre for Functional Materials and Nanotechnology (FMN), Institute of Science, Universiti Teknologi MARA (UiTM), Shah Alam, Selangor 40450, Malaysia*
[b]*Institute for Biodiversity and Sustainable Development, Universiti Teknologi MARA (UiTM), Shah Alam, Selangor 40450, Malaysia*
[c]*Faculty of Applied Sciences, Universiti Teknologi MARA (UiTM), Shah Alam, Selangor 40450, Malaysia*
[d]*Faculty of Applied Sciences, Universiti Teknologi MARA (UiTM), Sabah Branch Tawau Campus, Tawau, Sabah 91032, Malaysia*
[e]*Microwave Research Institute, Universiti Teknologi MARA (UiTM), Shah Alam, Selangor 40450, Malaysia*
[f]*Department of Physics, Faculty of Applied Sciences, Universiti Teknologi MARA (UiTM), Perak Branch Tapah Campus, Tapah Road, Perak 35400, Malaysia*
[g]*Pusat Pengurusan Makmal Alami & Fizikal UKM (ALAF-UKM), Aras 2, Kompleks Penyelidikan, Universiti Kebangsaan Malaysia, Bangi, Selangor 43600, Malaysia*
[h]*Faculty of Science and Marine Environment, Universiti Malaysia Terengganu, Kuala Nerus, Terengganu 21030, Malaysia*
[i]*Advanced Nano Materials (ANoMa) Research Group, Faculty of Science and Marine Environment, Universiti Malaysia Terengganu, Kuala Nerus, Terengganu 21030, Malaysia*
[j]*College of Pharmacy, King Saud University, Riyadh 11451, Kingdom of Saudi Arabia*
[k]*NANO-ElecTronic Centre, Faculty of Electrical Engineering, Universiti Teknologi MARA (UiTM), Shah Alam, Selangor 40450, Malaysia*
** Corresponding author. Tel.: +603-55444853; e-mail:syehdany@uitm.edu.my*

Received 15 September 2023, Revised 1 October 2025, Accepted 27 October 2025

ABSTRACT

This study reports the use of *Morinda citrifolia* leaf extract as a reducing and stabilizing agent in the green synthesis of tin oxide nanoparticles (SnO_2 NPs). Extract concentrations of 1:1, 1:3, 1:5, 1:7, and 1:10 were examined for the influence on the structural, optical, and chemical properties. XRD, FTIR, UV-DRS, and XPS were employed for characterization. XRD examination showed a tetragonal rutile structure with different crystalline extent, maximum at 1:3 extract ratio. Meanwhile, the formation of Sn-O-Sn and Sn-OH functional groups was verified by FTIR. UV-DRS revealed that the optical properties were tunable, ranging from 3.17 to 3.71 eV, and this depended on the extract concentration. XPS characterization of the optimal low-band-gap sample (1:10) confirmed the presence of Sn^{4+} and lattice oxygen. The study demonstrates that extract concentration significantly affects properties of SnO_2 NPs, highlighting the potential of *M. citrifolia* for eco-friendly nanoparticle synthesis.

Keywords: *Crystallinity, energy band gap, extract concentrations, Morinda citrifolia, tin oxide nanoparticles*

1. INTRODUCTION

In recent years, nanotechnology has gained significant prominence as a multidisciplinary research domain across various scientific and industrial sectors [1][2]. This rapid development is primarily driven by engineering advancements that allow precise and efficient manipulation of nanomaterials [3]. Due to their distinctive properties, including high physicochemical stability and an extensive surface area, nanoparticles have been extensively employed in numerous applications such as catalysis [4], biomedical sciences [5], energy [6], and optoelectronic devices [7], often offering superior performance compared to their bulk counterparts. Among the broad range of nanomaterials, metal oxide nanoparticles, particularly ZnO, TiO_2, CuO, Ag_2O, and SnO_2 which have received substantial attention owing to their high surface-to-volume ratios, tunable electronic band gaps, and excellent optical properties [8].

Among various metal oxide nanomaterials, tin oxide nanoparticles (SnO_2 NPs) stand out due to their wide band gap, typically ranging between 3.6 and 4.0 eV, and their classification as n-type semiconductors [9]. These nanoparticles exhibit high carrier concentrations up to 6 x 10^{20} cm^{-3}, attributed to oxygen vacancies that enhance electron density, thus making them suitable for a broad range of advanced applications [10]. SnO_2 NPs also offer additional advantages such as low cost, non-toxicity, high electron mobility ranging from 100 to 200 $cm^2V^{-1}s^{-1}$, notable photosensitivity, and excellent stability with high optical transmittance in the visible region [11][12]. Owing to these features, they are widely applied in solar energy conversion [13], chemical sensors [14], lithium-ion batteries[15], supercapacitors [16], and photocatalytic systems [17]. The efficiency of these applications is said to be strongly influenced by the structural uniformity and adjustable morphology of SnO_2 NPs, leading to a growing body of research focused on tailoring these characteristics to improve their sensitivity, selectivity, and response speed [18].

Multiple approaches can be used to synthesize SnO_2 NPs. Even though they are easy to perform, they tend to be costly, use dangerous substances, and may be difficult to implement at scale, such as the sol-gel process [19][20], laser ablation [21], chemical vapor deposition [22] and microwave [23]. While these methods are straightforward to execute, they come with expensive production costs, the use of dangerous chemicals, and problems with large-scale implementation. As a result, different ways to address the problem, like green synthesis, are becoming more popular. Green synthesis provides a more sustainable option for the synthesis of materials, and it uses techniques that are more in tune with the biological systems [24]. In this instance, plant extracts help transform metal salt precursors into nanoparticles, with phytochemicals like flavonoids, phenolics, terpenoids, and alkaloids serving multifunctionally as capping-reducing agents to metal ions and capping agents [25]. Afterward, the remaining phytochemicals adhere to the surfaces of the nanoparticles, and the functional groups ensure stabilization by inhibiting agglomeration and preventing direct interaction among the nanoparticle nuclei. Inhibiting the agglomeration and fusion of the nanoparticles helps to improve size control [26]. Employing natural extracts reduces negative environmental effects tied to traditional chemical methods, making the route safer, biocompatible, and eco-friendly [27]. Literature describes several studies focused on the green synthesis of SnO_2 NPs using different plant extracts, such as *Stevia rebaudiana* [28], Piper betle [29], *Chromaena odorata* [30], *Daphne alpina* [31], *Aloe barbadensis* [32], *Aquilaria malaccensis* [33], *Tradescantia spathacea* [34], *Pandanus amaryllifolius* [35], *Vernonia amygdalina* [36], and many more.

In this paper, the authors describe a straightforward, inexpensive, and eco-friendly method to synthesize SnO_2 NPs using *Morinda citrifolia* leaf extract as a reducing and capping agent for tin chloride (precursor salt), which contains hydroxyl-rich flavonoids [37][38]. This study seeks to assess how varying the concentration of the extract will affect the functional properties of the nanoparticles that have been synthesized, which have not been previously explored using this plant. Different concentrations of the extract can result in changes to the kinetics of reduction as well as the shape, size, stability, and overall characteristics of the resultant nanoparticles [39][40]. By optimizing the extract concentration, it is possible to enhance the quality and functional properties of the SnO_2 NPs. The extract concentration varied in five variations: 1:1, 1:3, 1:5, 1:7, and 1:10, whereby the precursor salt solution was maintained at constant concentration. The characterizations involve the utilization of several instruments: X-ray diffraction (XRD), Fourier transform infrared (FTIR), UV-Vis diffuse reflectance (UV-DRS), and X-ray photoelectron spectroscopy (XPS).

2. METHODOLOGY

2.1. Preparation of SnO_2 NPs

The methodology employed in this study was adapted from a previously reported procedure, with modifications in the precursor-to-extract ratios, which were extended to 1:7 and 1:10 [41]. *M. citrifolia* leaf extract was introduced gradually into a twirling solution of tin chloride (Sigma-Aldrich, 98% purity). A 1:1 volume ratio mixture was kept under continuous stirring at room temperature for three hours. Reaction was facilitated during this time. The colloidal suspension obtained was centrifuged, and the gelatinous precipitate obtained was dried for 12 hours at 50 °C. The dried product was calcined for three hours at 800 °C. This synthesis was repeated with different fill ratios of 1:3, 1:5, 1:7, and 1:10 for precursor and extract. The resulting products were then subjected to comprehensive characterization analyses.

2.2. Characterization

X-ray crystallographic analyses were performed utilizing an X'Pert PRO PANalytical X-ray diffractometer incorporating CuKα X-ray radiation (λ = 0.154 nm) at 45 kV and 40 mA. For a 2θ configuration of 5°-90°, a diffraction pattern for the specified configuration was produced at a scanning rate of 0.417782°/s. Estimation of the crystallite size was computed using the Debye–Scherrer equation predicated upon the full width at half maximum (FWHM) of the most intense diffraction peaks. Functional group analysis was performed using a PerkinElmer Spectrum 400 Fourier-transform infrared (FTIR) spectrometer with an ATR accessory. The 4000-400 cm^{-1} range of the sample was examined to identify distinctive Sn-O-Sn and Sn-OH vibrations, which allowed for the SnO_2 framework to be established. Evaluation of the sample optical properties made use of UV-Visible diffuse reflectance spectroscopy (UV-DRS) and a Varian Cary 5000 spectrophotometer. The reflectance data were analyzed to determine the optical band gap energy using the Kubelka–Munk function. X-ray photoelectron spectroscopy (XPS) analysis for elemental composition and corresponding chemical states of tin and oxygen was performed utilizing a Shimadzu/Kratos AXIS Ultra DLD system. Survey spectra were made with an acquisition resolution of 1.0 eV, and the high-resolution spectra were made at 0.1 eV and averaged over three scans to which were to improve accuracy.

3. RESULTS AND DISCUSSION

3.1. X-Ray Diffraction (XRD) Characterization

The X-ray diffraction patterns for different precursor salt-to-extract ratios for synthesized SnO_2 NPs in Figure 1a show well-defined diffraction peaks corresponding to the SnO_2 rutile tetragonal phase SnO_2. The peaks correspond to the standard JCPDS card no. 01-077-0452 data confirming the intended crystalline structure was formed. The center of the diffraction peaks that correspond to the (110), (101), (200), (211), (220), (002), (310), (112), (301), (202), (321) lattice planes were observed at 27.08°, 34.35°, 38.39°, 52.29°,

55.21°, 58.41°, 62.40°, 65.23°, 66.37°, 71.85°, and 79.83°, respectively. These findings are consistent with previous literature, further validating the structural integrity of the synthesized SnO_2 NPs [42][43].

The most prominent diffraction peaks were associated with the (110), (101) and (211) planes. The presence of all characteristic diffraction peaks across samples synthesized with varying precursor salt-to-extract ratios demonstrates a crystal lattice that shows a highly ordered atomic arrangement, confirming the successful formation of the SnO_2 crystalline framework. The absence of any extraneous peaks associated with impurities further validates the synthesis of pure, single-phase SnO_2 NPs. Pure SnO_2 NPs emerged from the synthesis, as no stray peaks from impurities cluttered the XRD patterns. The standout performer came from the 1:3 ratio of precursor salt to extract, where the diffraction peak hit its peak intensity and signaled top-notch crystallinity, probably due to the perfect balance of hydroxyl groups teaming up as dispersants [44]. They kept the particles apart, cutting down on clumps and boosting overall steadiness. This is the reason the (110) plane stood out sharp and bold, hinting at a tougher build for SnO_2 in that orientation over others. Later, the Debye-Scherrer equation (Equation 1) is applied to figure out the crystallite sizes (D). The analysis of both crystallite size and FWHM centered on the (110) plane, a common practice in SnO_2 studies due to this plane's high atomic density [45]. Equations (2-4) helped to calculate the interplanar spacing (d), dislocation density (δ), and lattice strain (ε) [46][47]. Table 1 lays out all these XRD details.

$$D = \frac{k}{\beta \, Cos} \quad (1)$$

$$d = \frac{\lambda}{2 \sin \theta} \quad (2)$$

$$\delta = \frac{1}{D^2} \quad (3)$$

$$\varepsilon = \frac{\beta}{4 \tan \theta} \quad (4)$$

The highest peak intensity is recorded for the sample with a 1:3 ratio, as shown in Figure 1b, which also exhibited the largest crystallite size among all samples measured at 33.43 nm. In the interim, the enlargements showing Figure 1c details on the (110) diffraction peak describe its positional and intensity variations. Increasing the extract concentration above 1:1 extends the 1:3 ratio through 1:10 as 2θ increments decrease on the diffraction peaks. Even with the observed shifts, SnO_2 NPs that were synthesized maintain their crystalline structure and phase purity. Meanwhile, Figure 1c presents an enlarged view of the relative shift and intensity of the (110) diffraction peaks. As the extract concentration increases beyond the 1:1 ratio, a noticeable shift in the diffraction peaks toward lower 2θ angles is observed for ratios ranging from 1:3 to 1:10. However, this shift does not significantly affect the crystalline structure or phase purity of the synthesized SnO_2 NPs. This behavior may be associated with variations in the lattice constant, influenced by stress within the crystal grains [48], as detailed in Table 1. When chelation between OH groups and Sn^{4+} ions is complete, the magnitude of the chelation bonding might differ with individual concentration. By increasing the extract volume, OH groups start fighting over capping duties, creating a messy chelation scene that leaves some Sn^{4+} ions exposed. Heat from calcination then pushes atoms around wildly, stretching bonds in unpredictable ways [49].

Yet crystallite size and FWHM refused to follow a straight path with rising extract levels. That clashes with studies on tomato extract from *Lycopersicon esculentum* [50] and *Camellia sinensis* [51], where more extract dialed down crystallinity and muddied the patterns. Here, the ups and downs show up in dislocation density and lattice strain, both tied to those shifts. Higher extract doses sparked swings in FWHM and size, pointing to patchy order in the crystal lattice, no matter what the ratio. Such chaos could ripple grain boundaries, where interface glitches stir the pot [52][53]. Furthermore, the variation in extract concentration may cause uneven capping of Sn^{4+} ions by hydroxyl groups, resulting in uneven bonding or steric hindrance. Such effects could contribute to inconsistent crystallite growth and irregular lattice dislocation, and strain.

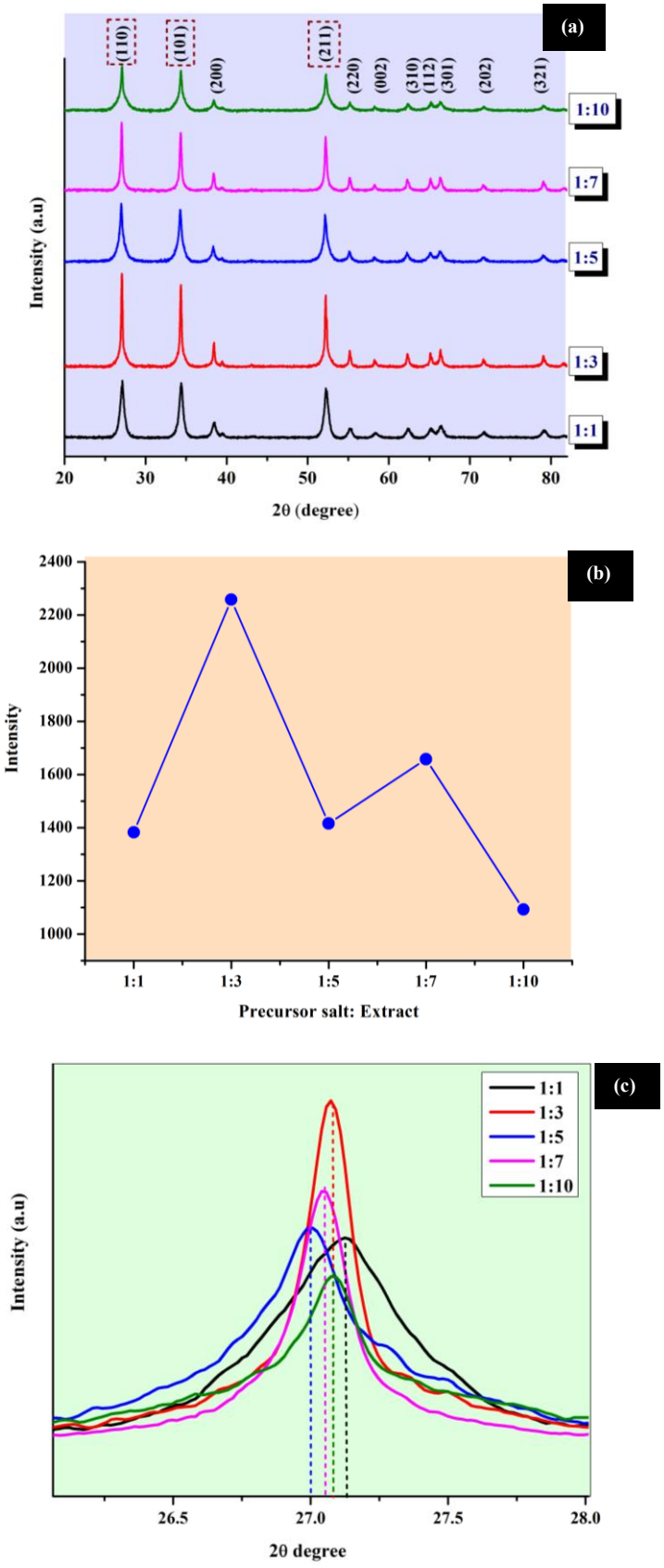

Figure 1. (a) XRD Profiles of SnO_2 NPs synthesized with varying precursor salt-to-extract ratios; (b) Magnified view of the (110) diffraction peaks; (c) Intensity of the (110) diffraction peaks at approximately 27.08°.

Table 1 XRD Parameters of SnO_2 NPs synthesized with different precursor salt-to-extract ratios

Parameter	Precursor salt: Extract				
	1:1	**1:3**	**1:5**	**1:7**	**1:10**
Crystallite size D (nm)	12.62	33.43	11.33	27.92	10.16
FWHM (°)	0.67	0.25	0.75	0.30	0.84
Lattice spacing (*d*)	0.3285	0.3289	0.3298	0.3292	0.3289
Dislocation density (δ)	0.0063	0.0009	0.0078	0.0013	0.0097
Lattice distortion (ε)	0.2379	0.0899	0.2660	0.1078	0.2959

3.2. Fourier Transform Infrared (FTIR) Spectroscopic Analysis

The FTIR spectra of SnO_2 NPs samples synthesized at different precursor salt-to-extract ratios (Figure 2) show two predominant clusters of absorption bands. The Sn-O-Sn asymmetric stretching vibrations are recorded in the range of 529 to 748 cm^{-1}, while the stretching vibration of the Sn-OH group appears between 921 and 1132 cm^{-1} [54][55]. These findings confirm the presence of key functional groups across all samples and validate the formation of the SnO_2 framework. Notably, the peaks corresponding to Sn-O-Sn groups are most intense at the 1:3 ratio, suggesting that this ratio yields the highest production of SnO_2 NPs. This enhancement may be attributed to an optimal capping effect from hydroxyl-rich flavonoids, which effectively stabilize Sn^{4+} ions during synthesis. In contrast, other ratios may result in weaker or inconsistent capping due to either an insufficient or excessive amount of hydroxyl groups.

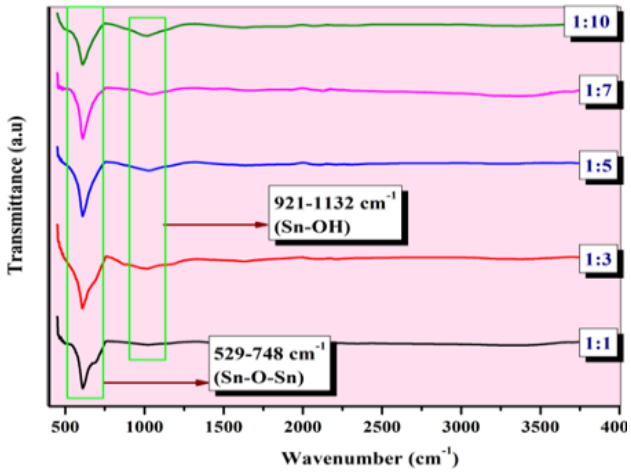

Figure 2. The FTIR spectra demonstrate the characteristic Sn-O-Sn asymmetric stretching vibrations, as well as the stretching modes corresponding to the Sn-OH groups.

3.3. UV-Vis Diffuse Reflectance (UV-DRS) Analysis

As shown in Figure 3a, all SnO_2 samples demonstrate visible spectrum reflectance edges between 450 and 480 nm. The employment of higher extract concentration induces a slight excitonic transition within the SnO_2 phase, resulting in a minor extension of the reflectance edge toward hypsochromic shift with variation of reflectance [56]. This reflects the previous analysis of XRD and FTIR, which contains variation in the parameter. It was observed that the highest reflectance percentages were recorded as 62 % for the ratio 1:1 and the lowest with 39 % using the ratio 1:7. This trend suggests that with higher extract concentrations, the reflectance might be reduced due to increased light absorption or more irregular surfaces.

Using the reflectance data, the Kubelka-Munk method utilized the reflectance data, whereby the square root of the function was plotted against the photon energy to obtain the optical band gap. The optical band gap was obtained by extrapolating the linear portion of the band gap graph to the energy axis intersection point [57]. As presented in Figure 3b, the band gap increases up to 3.71 eV at the 1:3 ratio before decreasing with the higher extract concentration. The 1:10 ratio provides the band gap of 3.17 eV, while the 1:3 ratio gives the maximum band gap of 3.71 eV as presented in Table 2. The obtained band gap values correlate with the changes in the linear graph dispersed in the optical band gap. The gap is less because of the crystal defects, which provide local energy position, and allow Sn^{4+} d-shell electron transition in the conduction band and valence band [58][59]. The increase in the gap, however, is plausible due to the quantum confinement effect [60].

Table 2 Reflectance and optical band gap values of SnO_2 NPs synthesized at different extract concentrations

Parameter	Precursor salt: Extract				
	1:1	**1:3**	**1:5**	**1:7**	**1:10**
Reflectance (%)	62	51	46	39	47
Energy band gap (eV)	3.61	3.71	3.27	3.33	3.17

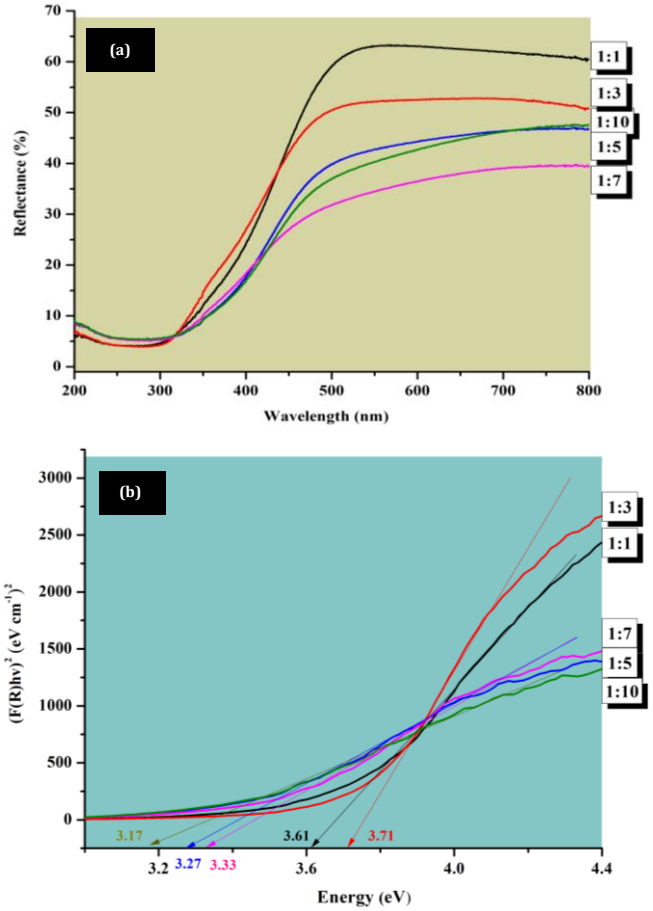

Figure 3. (a) Reflectance spectra and (b) Tauc plots of SnO_2 NPs synthesized with different extract concentrations.

3.4. X-ray Photoelectron Spectroscopy (XPS)

A decreased energy band gap can reduce the electron-transfer process from the valence band to the conduction one. Consequently, the SnO_2 1:10 sample, which had the smallest band gap (3.17 eV), was selected for study. The phase composition and chemical states of Sn and O elements were analyzed. The survey spectrum (Figure 4a) shows the presence of Sn, O, and C elements. It is evident that the high-resolution Sn 3d (Figure 4b) signal consists of two splitting peaks at the binding energy of 487.5 and 495.9 eV for Sn $3d_5/_2$ and Sn $3d_3/_2$, respectively, implying that tin in SnO_2 has a well-defined oxidation state. Additionally, for the O 1s XPS spectrum (Fig. 4c), a well-defined peak at 531.4 eV is observed, which can be assigned to lattice oxygen and its interaction with O_2 ions of the tetragonal structure formed by Sn^{4+} species. The synthesized SnO_2 NPs exhibited atomic concentrations of 49.66% for O 1s and 22.91% for Sn 3d. These findings are consistent with values reported in earlier studies [61][62].

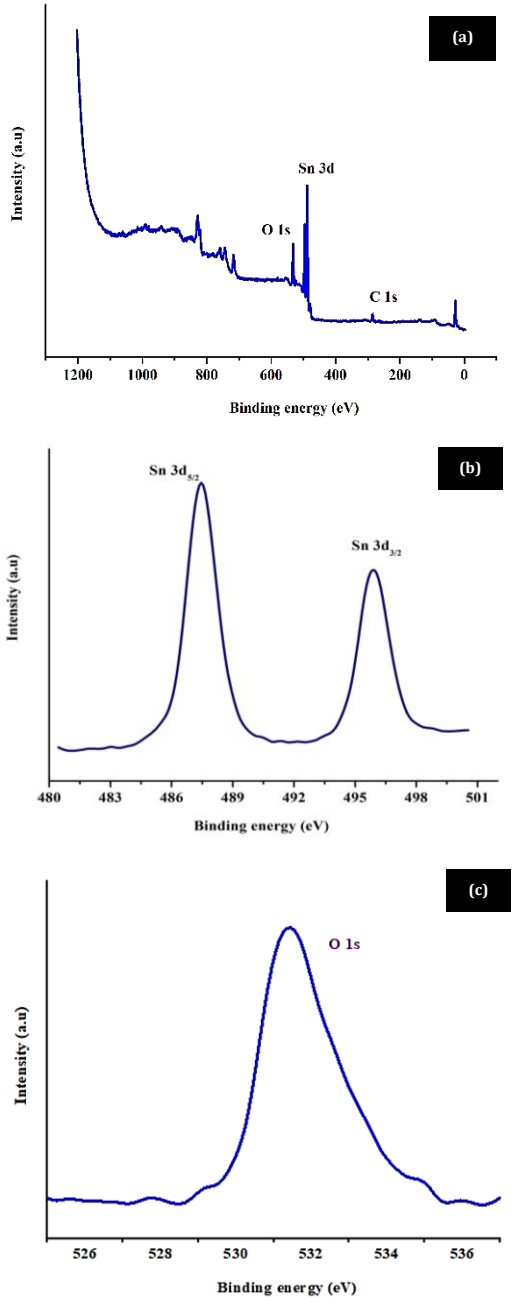

Figure 4. XPS analysis of SnO_2 NPs: (a) survey spectrum, (b) high-resolution Sn 3d peaks, and (c) O 1s peak for the sample synthesized at a 1:10 extract ratio.

4. CONCLUSION

Green synthesis of SnO_2 NPs using *M. citrifolia* leaf extract has been fully accomplished, with the extract concentration greatly impacting the characteristics of the resultant nanoparticles. The 1:3 precursor-to-extract ratio produced SnO_2 NPs with superior crystallinity, optimal Sn-O bonding, and the highest energy band gap (3.71 eV), indicating strong quantum confinement and minimal structural defects. Conversely, the 1:10 ratio showed a significant band gap reduction (3.17 eV), likely due to increased lattice disorder and oxygen vacancies. XRD, FTIR, UV-DRS, and XPS analyses consistently validated the formation of high-purity SnO_2 NPs with tunable optical and structural properties. This shows *M. citrifolia*'s great potential as a biodiversity secure and environmentally friendly means for the green synthesis of SnO_2 NPs with tailored functionalities suitable for applications in optoelectronics, sensors, and photocatalysis.

ACKNOWLEDGMENTS

Authors acknowledge the Universiti Teknologi MARA for funding under the Geran Insentif Penyelidikan Skim Q (GPQ) (600-RMC 5/3/GPQ (001/2023)).

REFERENCES

[1] S. A. Ahire, A. A. Bachhav, T. B. Pawar, B. S. Jagdale, A. V. Patil, and P. B. Koli, "The augmentation of nanotechnology era: A concise review on fundamental concepts of nanotechnology and applications in material science and technology," Results Chem, vol. 4, pp. 100633, 2022.

[2] S. Jadoun, R. Arif, and N. K. Jangid, "Green synthesis of nanoparticles using plant extracts: a review," Environ. Chem. Lett, vol. 19, pp. 355–374, 2021.

[3] V. Harish, M. M. Ansari, D. Tewari, A. B. Yadav, N. Sharma, S. Bawarig, M.-L. García-Betancourt, A. Karatutlu, M. Bechelany, and A. Barhoum, "Cutting-edge advances in tailoring size, shape, and functionality of nanoparticles and nanostructures: A review," J. Taiwan Inst. Chem. Eng, vol. 149, pp. 105010, 2023.

[4] Y. Han, J. Li, X. Zhang, and F. Xia, "Reversible down-regulation and up-regulation of catalytic activity of poly(N-isopropylacrylamide)-anchored gold nanoparticles," Nanotechnology, vol. 33, no. 16, pp. 165601, 2022.

[5] I. Buniyamin, R. Md Akhir, N. A. Asli, Z. Khusaimi, and M. F. Malek, "Nanotechnology applications in biomedical systems," Curr. Nanomater, vol. 17, pp. 167–180, 2022.

[6] H. S. Hussein, "The state of the art of nanomaterials and its applications in energy saving," Bull. Natl. Res. Cent, vol. 47, pp. 7, 2023.

[7] P. and P. Payal, "Role of nanotechnology in electronics: A review of recent developments and patents," Recent Pat. Nanotechnol, vol. 16, no. 1, pp. 45–66, 2022.

[8] W. Sadik, A. M. El-Demerdash, A. W. Nashed, A. A. Mostafa, and E. Lamie, "Synthesis and investigation of optical properties and enhancement photocatalytic activity of TiO2-SnO2 semiconductor for degradation of organic compounds," Sci. Rep, vol. 14, no. 27846, pp. 1-24, 2024.

[9] M. A. Dheyab, A. A. Aziz, M. S. Jameel, and N. Oladzadabbasabadi, "Recent advances in synthesis, modification, and potential application of tin oxide nanoparticles," Surfaces and Interfaces, vol. 28, pp. 101677, 2022.

[10] A. S. Yusuf, A. A. Abubakar, I. K. Mohammed, U. Ahmadu, and K. U. Isah, "A review of coating tin oxide electron transport layer for optimizing the performance of perovskite solar cells," Chem. Inorg. Mater, vol. 6, pp. 100100, 2025.

[11] M. S. G. K. Dalapati, H. Sharma, A. Guchhait, N. Chakrabarty, P. Bamola, Q. Liu, G. Saianand, A. M. S. Krishna, S. Mukhopadhyay, A. Dey, T. K. S. Wong, S. Zhuk, S. Ghosh, and S. Cha, "Tin oxide for optoelectronic, photovoltaic and energy storage devices: a review," J. Mater. Chem. A, vol. 9, pp. 16621, 2021.

[12] H. Sun, C. Yang, J. Xu, M. Cui, Y. Ren, W. Zhang, J. Zhao, and B. Liang, "Recent intensification strategies of SnO_2-based photocatalysts: A review," Chem. Eng. J, vol. 427, pp. 131564, 2022.

[13] J. Ye, Y. Li, A. A. Medjahed, S. Pouget, D. Aldakov, and Y. Liu, "Perovskite solar cells: Doped bilayer tin(IV) oxide electron transport layer for high open-circuit voltage planar perovskite solar cells with reduced hysteresis," Small, vol. 17, no. 5, pp. 2170020, 2021.

[14] E. Pargoletti, U. H. Hossain, I. D. Bernardo, H. Chen, T. Tran-Phu, G. L. Chiarello, J. Lipton-Duffin, V. Pifferi, and A. Tricoli, "Engineering of SnO_2-graphene oxide nanoheterojunctions for selective room-temperature chemical sensing and optoelectronic devices," ACS Appl. Mater. Interfaces, vol. 12, no. 35, pp. 39549–39560, 2020.

[15] F. Zoller, D. Böhm, T. Bein, and D. Fattakhova-Rohlfing, "Tin oxide-based nanomaterials and their application as anodes in lithium-ion batteries and beyond," ChemSusChem, vol. 12, pp. 4140–4159, 2019.

[16] S. Deepa, A. M. Philip, K. A. S. George, and Prasannakumari, "Microstructural, optical and dielectric variations in SnO_2 nanoparticles synthesized via surfactant-assisted sol–gel route," J. Mater. Sci.: Mater. Electron., vol. 44, pp. 283, 2021.

[17] I. Buniyamin, M. R. Mahmood, and Z. Khusaimi, "Utilization of tin oxide nanoparticles synthesized through plant-mediated methods and their application in photocatalysis: A brief review," Int. J. Chem. Biochem. Sci, vol. 24, pp. 116–123, 2023.

[18] Yu, Y. Dou, J. Zhao, S. Zhu, and K. Zhang, "A review of metal oxide semiconductors: Progress in solution-processed photovoltaic technologies," J. Alloys Compd, vol. 1024, pp. 180207, 2025.

[19] G. H. Patel, S. Chaki, R. Kannaujiya, Z. Parekh, A. B. Hirpara, and A. J. Khimani, "Sol-gel synthesis and thermal characterization of SnO_2 nanoparticles," Phys. B Condens. Matter, vol. 613, pp. 412987, 2021.

[20] L. E. Ahmadabad, F. S. Kalantari, H. Liu, A. Hasan, N. A. Gamasaee, Z. Edis, F. Attar, M. Ale-Ebrahim, F. Rouhollah, M. M. N. Babadaei, M. Sharifi, K. Shahpasand, K. Akhtari, M. Falahati, Y. Cai, "Hydrothermal method-based synthesized tin oxide nanoparticles: Albumin binding and antiproliferative activity against K562 cells," Mater. Sci. Eng. C, vol. 119, pp. 111649, 2021.

[21] U. M. Nayef, A. J. Hadi, S. K. Abdulridha, F. A.-H. Mutlak, and A. F. Ahmed, "Tin dioxide nanoparticles synthesized via laser ablation in various liquids medium," J. Opt, vol. 52, pp. 441–448, 2023.

[22] M. Gurgula, R. Zazpe, J. Rodriguez-Pereira, L. Hromadko, and J. M. Macak, "Improving photoelectrochemical performance of SnO_2 nanocones through TiOx shell via atomic layer deposition," Electrochim. Acta, vol. 519, pp. 145854, 2025.

[23] R. A. Tayeb, A. Alsafrani, and A. Khan, "Microwave-assisted synthesis and photoluminescence characterization of tetragonal rutile phase of SnO_2," Semiconductors, vol. 59, no. 4, pp. 318–327, 2025.

[24] N. Rani, P. Singh, S. Kumar, P. Kumar, and V. Bhankar, "Plant-mediated synthesis of nanoparticles and their applications: A review," Mater. Res. Bull, vol. 163, pp. 112233, 2023.

[25] I. Buniyamin, M. F. A. Halim, K. A. Eswar, K. J. Jalani, S. A. I. A. Syed Abd Kadir, M. Mohammad, M. Y. Idorus, N. A. Asli, and M. R. Mahmood, "Natural biomolecules in leaves and fruit extracts mediate the biosynthesis of SnO_2 nanoparticles: A mini review," Int. J. Pharm. Nutraceut. Cosmet. Sci, vol. 6, no. 2, pp. 24–40, 2023.

[26] S. Sagadevan, J. A. Lett, I. Fatimah, Y. Lokanathan, M. M. H., and M. R. J. W. C. Oh, "Current trends in the green syntheses of tin oxide nanoparticles and their biomedical applications," Mater. Res. Express, vol. 8, pp. 082001, 2021.

[27] V. Soni, P. Raizada, P. Singh, H. N. Cuong, R. S., A. Saini, R. V. Saini, Q. V. Le, A. K. Nadda, and T.-T. Le, "Sustainable and green trends in using plant extracts for the synthesis of biogenic metal nanoparticles toward environmental and pharmaceutical advances: A review," Environ. Res, vol. 202, pp. 111622, 2021.

[28] M. G. T. Nathan and P. Myvizhi, "Green Synthesis and Characterization of Tin Oxide Nanoparticles Using Plant Extract," Int. J. Pure Appl. Math, vol. 119, pp. 6439–6448, 2018.

[29] Singha, N. Kaura, P. Kaur, S. Kaur, P. Kukkar, V. Kumar, and D. Kukkar, "Piper betle leaves mediated synthesis of biogenic SnO_2 nanoparticles for photocatalytic degradation of reactive yellow 186 dye under direct sunlight," Environ. Nanotechnol. Monit. Manag, vol. 10, pp. 1–9, 2018.

[30] I. Buniyamin, N. A. Asli, K. A. Eswar, S. A. I. A. Syed Abd Kadir, A. Saiman, M. Y. Idorus, M. R. Mahmood, and Z. Khusaimi, "Biosynthesis of tin(IV) oxide nanoparticles (SnO_2 NPs) via Chromolaena Odorata leaves: The Influence of heat on the extraction procedure," J. Sci. Math. Lett, vol. 12, no. 2, pp. 142–150, 2024.

[31] S. Haq, W. Rehman, M. Waseem, M. Shahid, K. H. S., and M. Nawaz, "Adsorption of Cd^{2+} ions on plant mediated SnO_2 nanoparticles," Mater. Res. Express, vol. 3, pp. 105019, 2016.

[32] A. Ayeshamariam, T. M. Begam, J. M. Jayachandran, P. K. G. Praveen Kumar, and M. Bououdina, "Green synthesis of nanostructured materials for antibacterial and antifungal activities," Int. J. Bioassays, vol. 2, no. 1, pp. 304–311, 2013.

[33] I. Buniyamin, N. A. Asli, F. S. Husairi, K. A. Eswar, M. Mohammad, M. Rusop, and Z. Khusaimi, "The photocatalytic characteristics of tin oxide nanoparticles synthesized through Aquilaria malaccensis," Int. J. Chem. Biochem. Sci, vol. 24, no. 7, pp. 63–73, 2023.

[34] S. N. Matussin, M. H. Harunsani, A. L. Tan, A. Mohammad, M. H. Cho, and M. M. Khan, "Photoantioxidant studies of SnO_2 nanoparticles fabricated using aqueous leaf extract of Tradescantia spathacea," Solid State Sci, vol. 105, pp. 106279, 2020.

[35] I. Buniyamin, R. M. Akhir, M. Z. Nurfazianawatie, H. Omar, N. S. A. Malek, N. F. Rostan, K. A. Eswar, N. F. Rosman, M. A. Abdullah, N. A. Asli, Z. Khusaimi, and M. Rusop, "Aquilaria malaccensis and Pandanus amaryllifolius mediated synthesis of tin oxide nanoparticles: The effect of the thermal calcination temperature," Mater. Today Proc, vol. 75, pp. 23–30, 2023.

[36] N. Awoke, D. Pandey, and A. B. Habtemariam, "Synthesis of tin(IV) oxide nanoparticles using plant leaf extracts of Vernonia amygdalina and Mentha spicata," Regen. Eng. Transl. Med, vol. 8, pp. 407–412, 2021.

[37] S. Sang, X. Cheng, N. Zhu, R. E. Stark, V. Badmaev, G. Ghai, and R. T. R. and C.-T. H., "Flavonol glycosides and novel iridoid glycoside from the leaves of Morinda citrifolia," J. Agric. Food Chem, vol. 49, pp. 4478–4481, 2001.

[38] H. Setyani and H. Setyowati, "Phytochemical investigation of noni (Morinda citrifolia L.) leaves extract applicated for sunscreen product," Malaysian J. Fundam. Appl. Sci, pp. 164–167, 2018.

[39] I. V. Makarov, A. J. Love, O. V. Sinitsyna, S. S. Makarova, N. O. Kalinina, and M. E. Taliansky, "'Green' nanotechnologies: Synthesis of metal nanoparticles using plants," Acta Naturae, vol. 6, no. 1, pp. 35–44, 2014.

[40] Y. V. S. Oliveira, M. M. R. Azevedo, C. A. Felsemburgh, J. de Souza, A. K. O. Lima, H. C. Braga, D. B. Tada, K. Gul, G. Nakazato, and P. S. Taube, "Green synthesis of silver nanoparticles from cumaru (Dipteryx odorata) leaf extract," Discover Applied Sciences, vol. 7, pp. 227, 2025.

[41] I. Buniyamin, N. A. Asli, R. Md Akhir, S. M. Jafar, K. A. Eswar, M. K. A. Mahmood, M. Y. Idorus, M. S. Shamsudin, A. F. M. M. Rahman, M. R. Mahmood, and Z. Khusaimi, "Biofabricated SnO_2 nanoparticles derived from leaves extract of Morinda citrifolia and Pandanus amaryllifolius for photocatalytic degradation," J. Clust. Sci, vol. 36, pp. 3, 2025.

[42] F. Is, G. Purwiandono, M. H. Jauhari, A. A. A. P. Maharani, S. Sagadevan, W.-C. Oh, and R.-A. Doong, "Synthesis and control of the morphology of SnO2 nanoparticles via various concentrations of Tinospora cordifolia stem extract and reduction methods," Arab. J. Chem, vol. 15, pp. 103738, 2022.

[43] G. Ramanathan and K. R. Murali, "Photocatalytic activity of SnO2 nanoparticles," J. Appl. Electrochem, vol. 52, pp. 849–859, 2022.

[44] N. Bahari, N. Hashim, K. Abdan, A. Md Akim, and B. M. Al-Shdifat, "Role of honey as a bifunctional reducing and capping/stabilizing agent: Application for silver and zinc oxide nanoparticles," Nanomaterials, vol. 13, pp. 1244, 2023.

[45] J. T. Wang, X. L. Shi, W. W. Liu, X. H. Zhong, J. N. Wang, L. Pyrah, K. D. Sanderson, P. M. Ramsey, and M. Hirata, "Influence of preferred orientation on the electrical conductivity of fluorine-doped tin oxide films," Sci. Rep, vol. 4, pp. 3679, 2014.

[46] N. F. H. Zambri, E. Yusrianto, N. Marsi, and I. A. Manaf, "Phase formation and microstructure properties of autoclaved aerated concrete (AAC) based on ceramic and gypsum waste (CGW) as raw material addition," J. Adv. Res. Micro Nano Eng, vol. 30, no. 1, pp. 10–21, 2024.

[47] H. Köse, Ş. Karaal, A. O. Aydin, and H. Akbulut, "Structural properties of size-controlled SnO_2 nanopowders produced by sol-gel method," Materials Science in Semiconductor Processing, vol. 38, pp. 404–412, 2015.

[48] N. Motloung, S. V. Tsega, M. Dejene, H. C. Swart, H. M. Om, L. F. Koao, and T. E. Motaung, "Effect of annealing temperature on structural and optical properties of ZnAl2O4: 1.5% Pb2+ nanocrystals synthesized via sol-gel reaction," J. Alloy Compd, vol. 677, pp. 72–79, 2016.

[49] M. K. Hussen and F. B. Dejene, "Influence of annealing temperature on material properties of red emitting $ZnGa_2O_4$:Cr^{3+} nanostructures," J. Sol-Gel Sci. Technol, vol. 88, pp. 454–464, 2018.

[50] H. E. Garrafa-Galvez, O. Nava, C. A. Soto-Robles, A. R. Vilchis-Nestor, A. Castro-Beltrán, and P. A. Luque, "Green synthesis of SnO_2 nanoparticle using Lycopersicon esculentum peel extract," J. Mol. Struct, vol. 1197, pp. 354-360, 2019.

[51] M. P. A. Luque, M. J. Chinchillas-Chinchillas, O. Nava, E. Lugo-Medina, L. E. Martínez-Rosas, A. Carrillo-Castillo, A. R. Vilchis-Nestor, H. E. Garrafa-Galvez, and E. Madrigal-Muñoz, "Green synthesis of tin dioxide nanoparticles using Camellia sinensis and its application in photocatalytic degradation of textile dyes," Int. J. Light Electron Opt, vol. 229, pp. 166259, 2021.

[52] S. Manir, "Size-strain distribution analysis from XRD peak profile of (Mg, Fe) co-doped SnO2 nanoparticles fabricated using chemical co-precipitation route," Ceram. Int, vol. 50, no. 21, pp. 44038–44055, 2024.

[53] R. Verma, A. Chauhan, Neha, K. M. Batoo, R. Kumar, M. Hadhi, and E. H. Raslan, "Effect of calcination temperature on structural and morphological properties of bismuth ferrite nanoparticles," Ceram. Int, vol. 47, pp. 3680–3691, 2021.

[54] H. E. Quintero González, E. L. Medina, R. V. Quevedo Robles, H. E. Garrafa Gálvez, Y. A. Baez Lopez, E. V. Viveros, F. A. Molina, A. R. Vilchis Nestor, and P. A. Luque Moral, "A study of the optical and structural properties of SnO_2 nanoparticles synthesized with Tilia cordata applied in methylene blue degradation," Symmetry, vol. 14, pp. 2231, 2022.

[55] G.-B. Hong and C.-J. Jiang, "Synthesis of SnO2 nanoparticles using extracts from Litsea cubeba fruits," Mater. Lett, vol. 194, pp. 164–167, 2017.

[56] T. S. Suresh Sagadevan, J. Anita Lett, S. F. Alshahateet, I. Fatimah, G. K. Weldegebrieal, M.-V. Le, S. Paiman, and E. Leonard, "Photocatalytic degradation of methylene blue dye under direct sunlight irradiation using SnO_2 nanoparticles," Inorg. Chem. Commun, vol. 141, pp. 109547, 2022.

[57] I. Buniyamin, Z. Khusaimi, N. A. Asli, K. A. Eswar, M. R. Mahmood, S. A. I. A. S. A. Kadir, A. Saiman, M. Y. Idorus, and A. R. A. Razak, "The application of pandan and soybean extracts on the biosynthesis of tin oxide nanoparticles," J. Sci. Math. Lett, vol. 12, no. 2, pp. 83–92, 2024.

[58] N. M. Al-Hada, H. M. Kamari, A. A. Baqer, A. H. Shaari, and E. Saion, "Thermal calcination-based production of SnO_2 nanopowder: an analysis of SnO_2 nanoparticle characteristics and antibacterial activities," Nanomaterials, vol. 8, pp. 250, 2018.

[59] B. P. Narasaiah, P. Banoth, A. Sohan, B. K. Mandal, A. G. Bustamante Dominguez, L. D. L. S. Valladares, and P. Kollu, "Green biosynthesis of tin oxide nanomaterials mediated by agro-waste cotton boll peel extracts for the remediation of environmental pollutant dyes," ACS Omega, vol. 7, pp. 15423–15438, 2022.

[60] G. Kiruthiga, K. S. Rajni, N. Geethanjali, T. Raguram, E. Nandhakumar, and N. Senthilkumar, "SnO_2: Investigation of optical, structural, and electrical properties of transparent conductive oxide thin films prepared by nebulized spray pyrolysis for photovoltaic applications," Inorg. Chem. Commun, vol. 145, pp. 109968, 2022.

[61] Y. Etafa, T. K. Sarma, and T. K. Sahu, "Phytosynthesis and characterization of tin-oxide nanoparticles (SnO_2-NPs) from Croton macrostachyus leaf extract and its application under visible light photocatalytic activities," Sci. Rep, vol. 14, pp. 10780, 2024.

[62] A. Phukan, R. P. Bhattacharjee, and D. K. Dutta, "Stabilization of SnO_2 nanoparticles into the nanopores of modified Montmorillonite and their antibacterial activity," Adv. Powder Technol, vol. 28, pp. 139–145, 2017.